Carbon-13 NMR Method for the Detection of Correlated Hydrogen Exchange at Adjacent Backbone Peptide Amides and Its Application to Hydrogen Exchange in Five Antiparallel β Strands within the Hydrophobic Core of *Streptomyces* Subtilisin Inhibitor (SSI)[†]

Kenichi Uchida,[‡,§] John L. Markley,[‖] and Masatsune Kainosho*,[‡,⊥]

Graduate School of Science, Tokyo Metropolitan University, 1-1 Minami-ohsawa, Hachioji, Tokyo 192-0397, Japan, and National Magnetic Resonance Facility at Madison, Biochemistry Department, University of Wisconsin−Madison, Madison Wisconsin 53706

ABSTRACT: A novel method for monitoring proton−deuteron (H/D) exchange at backbone amides is based on the observation of H/D isotope effects on the ^{13}C NMR signals from peptide carbonyls. The line shape of the carbonyl $^{13}C_i$ signal is influenced by differential H/D occupancy at the two adjacent amides: the H^N_{i+1} (β site) and the H^N_i (γ site). At a carbon frequency of 75.4 MHz, the H → D isotope shifts on the ^{13}C signal are about 5−7 Hz for exchange at the β site and 2 Hz or less for exchange at the γ site. Because the effects at the two sites are additive, the time dependence of the line shape of a particular carbonyl resonance can report not only the exchange rates at the individual sites but also the level of dual exchange. Therefore, the data can be analyzed to determine the rate (k_c) and degree of correlated exchange ($X_{\beta\gamma}$) at the two sites. We have applied this approach to the investigation of the pH dependence of hydrogen exchange at several adjacent residues in *Streptomyces* subtilisin inhibitor (SSI). Two selectively labeled SSI proteins were produced: one with selective $^{13}C'$ labeling at all valyl residues and one with selective $^{13}C'$ labeling at all leucyl residues. This permitted the direct observation by one-dimensional ^{13}C NMR of selected carbonyl signals from residues with slowly exchanging amides at the i and $i + 1$ positions. The residues investigated were located in an α helix and in a five-stranded antiparallel β sheet. Samples of the two labeled proteins were prepared at various pH* values, and ^{13}C NMR spectra were collected at 50 °C prior to and at various times after transferring the sample from H_2O to ^2H_2O. Most of the slowly exchanging amides studied were intramolecular hydrogen-bond donors. In agreement with prior studies, the results indicated that the exchange rates of the amide hydrogens in proteins are governed not only by hydrogen bonding but also by other factors. For example, the amide hydrogen of Thr34 exchanges rapidly even though it is an intramolecular hydrogen-bond donor. Over nearly the whole pH range studied, the apparent rates of uncorrelated exchange (k_β and k_γ) were proportional to $[OH^-]$ and the apparent rates of correlated exchange at two adjacent sites (k_c) were roughly proportional to $[OH^-]^2$. This enabled us to extract the pH-independent exchange rates ($k_\beta°$, $k_\gamma°$, and $k_c°$). In all cases in which correlated exchange could be measured, the observed sigmoidal pH dependence of $X_{\beta\gamma}$ could be replicated roughly from the derived pH-independent rates.

The internal fluctuations of protein molecules are deeply related to their structure and stability and contribute to their functions. Protein fluctuations have been studied extensively by many methods (*1*). One of the most important approaches has been to measure exchange rates of labile hydrogens, including the backbone amide hydrogens (*2*). A wide variety of studies have reported the use of these hydrogens as structural probes (*3*, *4*). Hydrogen exchange also has been used to detect intermediates during protein folding (*5−8*) or interactions between proteins and other molecules (*9−11*). The exchange rates of the backbone amide hydrogens have been measured by many methods, such as ultraviolet spectroscopy (*12*) and infrared spectroscopy (*13*, *14*), without regard to their location in proteins. Advances in high-resolution nuclear magnetic resonance (NMR)[1] spectroscopy have enabled the measurement of exchange rates of individual amide hydrogens in a site-specific manner (*15*, *16*). Thus, it has become possible to obtain detailed information about the dynamic structure of proteins. Exchange occurs not only at amides located near the surface of the protein molecule but also at those fully buried in the interior of the

---

* To whom correspondence should be addressed. Telephone: +81-426-77-2544. Fax: +81-426-77-2544. E-mail: kainosho@nmr.chem.metro-u.ac.jp.
‡ Tokyo Metropolitan University.
§ Present address: Department of Biosciences, School of Science and Engineering, Teikyo University, 1-1 Toyosatodai, Utsunomiya 320-8551, Japan.
‖ University of Wisconsin−Madison.
⊥ CREST of Japan Science and Technology Agency (JST).

protein, even though they appear to be inaccessible to solvent molecules in static structural models derived from X-ray crystallography or NMR spectroscopy (*17*). The exchange rates of amide hydrogens in proteins are often very slow, and it is not uncommon for the rates to be reduced by several orders of magnitude, as compared to those of free small peptides. To explain the remarkable reduction of the exchange rates, several factors have been proposed, such as hydrogen bonding, the effect of secondary structures, the depth from the surface of the protein molecule, the solvent accessibility, and so on. All of these factors are important, but none of them is definitive; therefore, the reasons for the slower exchange rates are still unclear (*18*). It is important to consider the mechanisms of exchange in studying the relationship between internal fluctuations and the amide hydrogen exchange rates. The proposed models for exchange may be divided in two general categories: the solvent penetration model (*19*) or expansile cavity model (*20*) and the local unfolding model (*21, 22*). The former does not easily explain the correlated exchange of the amide hydrogens, which is observed under certain conditions. Correlated exchange requires a large conformational change, almost to the point of denaturation, and such global unfolding has been reported in some cases (*23−25*). Internal motions, such as global unfolding, have been studied indirectly by the pH dependence of the exchange rates; however, more details can be obtained if correlated exchange is detected directly. Correlated exchange of the amide hydrogens in the β sheet of BPTI was detected by measuring NOEs observed between pairs of amide hydrogens, as a function of the extent of H/D exchange (*23, 26*). Miranker et al. (*27*) applied electrospray ionization mass spectrometry to lysozyme, to distinguish the exchange mechanisms from the line shapes of the molecular ion peaks caused by partial deuteration. In addition, a method has been reported for determining the exchange mechanism from mass spectrometric identification of the distribution of the molecular weights of enzymatic fragments of a protein undergoing H/D exchange (*28*).

In this paper, we report a new method for the measurement of amide hydrogen exchange rates and correlated exchange
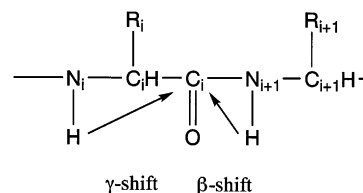

FIGURE 1: H/D exchange at positions i (γ site) and $i + 1$ (β site) can lead to isotope effects on the NMR chemical shift of the carbonyl carbon $^{13}C_i$. Typical values of these isotope effects at 75.4 MHz are 5−6 Hz for H/D exchange at the β site and about 2 Hz for H/D exchange at the γ site (*30, 36*).
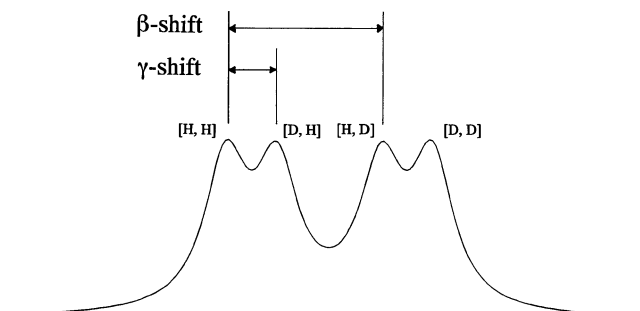

FIGURE 2: Simulated line shape for carbonyl carbon resonance $^{13}C'_i$ with partially exchanged neighboring amide hydrogens at positions i and $i + 1$. The four peaks originate from various [$i, i + 1$] isotopomers: from left to right, [H,H], [D,H], [H,D], and [D,D]. The simulation assumed slow exchange on the chemical-shift time scale, β shift = 6 Hz, γ shift = 2 Hz, and line width = 1 Hz.

occurring at adjacent residues. The method utilizes selective ^{13}C labeling and direct ^{13}C signal detection (*29−31*). The approach takes advantage of isotope effects from the neighboring amide hydrogens on the carbonyl ^{13}C chemical shift (*32*). H/D exchange at two amide hydrogens, H^N_{i+1} (β site) and H^N_i (γ site), can induce isotope effects on the carbonyl carbon resonance of the ith residue (Figure 1). When a protein prepared in H_2O is dissolved in ^2H_2O, the amide protons will start to exchange with deuterons. The chemical shift of the carbonyl ^{13}C NMR resonance moves to a higher field, when the neighboring amide proton is replaced with deuteron. The typical H/D isotope effects at 75.4 MHz are 5−7 Hz for the β shift and 2 Hz or less for the γ shift (*30, 33*). Because the isotope effects from the neighboring amide hydrogens have different values, up to four peaks can be observed for each carbonyl carbon. These peaks are derived from the isotopomers, which have different combinations of protons (H) and/or deuterons (D) at the two sites (Figure 2). These species are represented by [H,H], [D,H], [H,D], and [D,D], in which the first and second letters in the brackets indicate the isotopes occupying the γ and β sites, respectively. Under conditions of slow exchange, the populations of the four species can be derived from their respective peak areas and the method can be used to determine not only the exchange rates at the individual β and γ sites but also the rate of correlated exchange at the two sites. Under intermediate or fast exchange conditions, the line shape no longer provides separate information about the four sites.
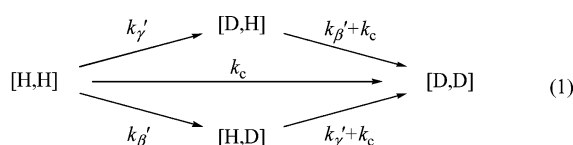
We have applied this method to the investigation of the pH dependence of H/D exchange in *Streptomyces* subtilisin inhibitor (SSI). SSI is a homodimeric serine protease inhibitor (23 kDa for the dimer). The two subunits of SSI face one other, with a five-stranded β sheet at the interface. The

dimeric structure of SSI is very stable; the dissociation constant to the monomers is estimated to be below 5×10^{-7} M at pH 7 (*34*). The structural and functional features of SSI have been studied by many methods (*35*). SSI is known to have remarkably slowly exchanging amide hydrogens (*24, 36*) that are amenable to study by observation of the ^{13}C NMR signals from samples labeled selectively by incorporation of [$^{13}C'$-Leu] or [$^{13}C'$-Val]. The slowly exchanging amide hydrogens of SSI were found to be concentrated on the five-stranded β sheet. We report here the pH dependence of noncorrelated and correlated H/D exchange at six adjacent residues in SSI. In addition, we have investigated noncorrelated exchange at another four adjacent residues in SSI.

MATERIALS AND METHODS

When a protein sample prepared in H_2O is dissolved in ^2H_2O, adjacent amide protons exchange to deuterons according to the pathway,

$$
\begin{array}{ccc}
 & \xrightarrow{k_\gamma'} [D,H] \xrightarrow{k_\beta'+k_c} & \\
[H,H] & \xrightarrow{k_c} & [D,D] \\
 & \xrightarrow[k_\beta']{} [H,D] \xrightarrow[k_\gamma'+k_c]{} &
\end{array}
\tag{1}
$$

If a large excess of ^2H_2O is present, then the reverse reaction will be negligible. In eq 1, k_β' and k_γ' are the exchange rate constants for the β and γ sites in the process whereby amide hydrogens exchange independently and never simultaneously. In the correlated exchange process, characterized by the rate constant k_c, both the β and γ sites exchange "simultaneously" (during the same unfolding step). Species [D,H] and [H,D] are only produced in a stochastic manner, but [D,D] is produced not only by the two sequential stochastic process but also by the correlated process. In this way, the time dependence of the four species can be analyzed to yield the uncorrelated exchange rates of the neighboring amide hydrogens (k_β and k_γ) and the rate of correlated exchange at the two adjacent sites (k_c). The rate constant k_c accounts for the excess build-up of [D,D] that cannot be accounted by the sum (k_β and k_γ).

The time dependence of the populations of the four species can be expressed as

$$
[H,H] = [H,H]_0 e^{-(k_\beta'+k_\gamma'+k_c)t}
\tag{2}
$$

$$
[D,H] = [H,H]_0 \{ e^{-(k_\beta'+k_c)t} - e^{-(k_\beta'+k_\gamma'+k_c)t} \}
\tag{3}
$$

$$
[H,D] = [H,H]_0 \{ e^{-(k_\gamma'+k_c)t} - e^{-(k_\beta'+k_\gamma'+k_c)t} \}
\tag{4}
$$

$$
[D,D] = [H,H]_0 - [H,H] - [D,H] - [H,D]
\tag{5}
$$

where $[H,H]_0$ is the initial population of the [H,H] species. These equations represent the behavior of populations of the four species completely. In the actual analysis, these equations are integrated by the accumulation period. The apparent exchange rate constants of the β and γ sites are represented by

$$
k_\beta = k_\beta' + k_c
\tag{6}
$$

$$
k_\gamma = k_\gamma' + k_c
\tag{7}
$$

The fraction of H/D exchange at the β and γ sites occurring by the correlated mechanism, $X_{\beta\gamma}$, is defined by

$$
X_{\beta\gamma} = \frac{2k_c}{k_\beta' + k_\gamma' + 2k_c}
\tag{8}
$$

with $0 \leq X_{\beta\gamma} \leq 1$. The limiting case of $X_{\beta\gamma} = 0$ means that no correlated exchange occurred, and $X_{\beta\gamma} = 1$ indicates that all of the exchange occurred in a correlated manner.

Preparation of Isotopically Labeled Amino Acids and SSIs. [1-^{13}C]-DL-leucine and [1-^{13}C]-DL-valine were prepared from Na^{13}CN and isovaleraldehyde and isobutyraldehyde, respectively, by Bucherer's method. The ^{13}C-labeled SSIs were prepared by aerobic fermentation of *Streptomyces albogriseolus* S-3253, obtained from Prof. Murao at Osaka Prefectural University, in a medium containing an amino acid mixture in which the desired normal amino acid was replaced by the isotopically labeled one as described in a previous paper (*29*).

^{13}C NMR Spectroscopy. All ^{13}C NMR spectra were recorded on a Varian XL-300 spectrometer at a ^{13}C frequency of 75.4 MHz under the condition of full ^1H decoupling by MLRV16. The time-dependent amide hydrogen exchange experiments were carried out as follows. Lyophilized labeled SSI (20 mg) was dissolved in 0.5 mL of water, and the pH was adjusted by adding small amounts of dilute HCl or NaOH. After incubation for 1 h at 60 °C, the pH value was confirmed. If the meter reading was considerably different from the desired value, then the pH was readjusted. Then, the solution was lyophilized. The sample was dissolved in 0.5 mL of ^2H_2O at 0 °C as rapidly as possible, with avoidance of moisture, and then ^{13}C NMR spectra were collected at 50 °C as a function of time. The pH* value of each sample was measured just before and after the NMR measurement to confirm that it had not changed significantly. The delay in collecting the first data set for each sample was about 10 min. The spectral width (about 1 kHz) covered only the carbonyl region, and 4 k of time-domain data were collected. Each time-domain data set was the average of 1024 FID transients, and the accumulation time was 34 min. All data sets were subjected to a 0.5 Hz line broadening function and were Fourier-transformed to yield a spectrum consisting of 8 k data points. Data were collected until the intensities of the [H,H] and [D,D] peaks were almost equal.

Determination of the Exchange Rate Constants and the Fraction of Correlated Exchange. The exchange rate constants k_β', k_γ', and k_c were determined from total line-shape analysis by the nonlinear least-squares method. In the analysis, we made three, generally accepted assumptions: (1) the exchange to deuteron from hydrogen does not reverse, because there is a large excess of ^2H_2O over H_2O; (2) the lifetimes of the four isotopomeric species are sufficiently long, relative to the NMR time scale, that the chemical shifts and the line widths are independent of the exchange rates; and (3) the line shapes of the resonances are Lorentzian. To carry out the line-shape analysis, subspectra containing only one or two (if the signals overlapped) carbonyl resonances were extracted from a time series of ^{13}C NMR spectra. In most cases, each time point represented the summation over an appropriate time interval for obtaining a high signal-to-noise ratio. The resonance lines were fitted by Lorentzian functions, and the intensities of the four species were

calculated by time averaging, from eqs 2 to 5. Namely, the fitting functions are represented as follows:

$$\overline{[\mathrm{H,H}]} = [\mathrm{H,H}]_0 \int_{t_1}^{t_1+\Delta t} (e^{-(k_{\beta}'+k_{\gamma}'+k_c)t})\mathrm{d}t \qquad (9)$$

$$\overline{[\mathrm{D,H}]} = [\mathrm{H,H}]_0 \int_{t_1}^{t_1+\Delta t} (e^{-(k_{\beta}'+k_c)t} - e^{-(k_{\beta}'+k_{\gamma}'+k_c)t})\mathrm{d}t \quad (10)$$

$$\overline{[\mathrm{H,D}]} = [\mathrm{H,H}]_0 \int_{t_1}^{t_1+\Delta t} (e^{-(k_{\gamma}'+k_c)t} - e^{-(k_{\beta}'+k_{\gamma}'+k_c)t})\mathrm{d}t \quad (11)$$

$$\overline{[\mathrm{D,D}]} = [\mathrm{H,H}]_0\Delta t - \overline{[\mathrm{H,H}]} - \overline{[\mathrm{D,H}]} - \overline{[\mathrm{H,D}]} \qquad (12)$$

The bars above species names indicate the time-averaged concentrations over the accumulation period (Δt). The chemical shifts and the line widths were fixed in the calculation. The nonlinear least-squares program, which used the modified Marquardt method (*37*), was written in BASIC language and run on a personal computer. The exchange rates at the γ and β sites and their degrees of correlation were calculated from eqs 6 to 8.

RESULTS

Amide Hydrogen Exchange Rates and the Degree of Correlation in SSI. Typical results from H/D investigations of [L]SSI and [V]SSI are shown in Figure 3. The assignments of these carbonyl resonances (residue numbers shown at the bottom of the figure) were determined primarily by the [15]N-^{13}C double-labeling method (*29*). The details of the assignments will be reported elsewhere. Residues were classified into three groups based on the time dependence of their $^{13}\mathrm{C}_i'$ signals. The first group constituted residues that showed no time-dependent spectral changes: Leu6, Val20, Val56, Leu60, Leu63, Val69, Val74, and Val110. The $^{13}\mathrm{C}'$ chemical shifts of these residues did not change even when the sample was incubated for 1 h at 60 °C, and therefore, both of the neighboring amide hydrogens of these carbonyl carbons had exchanged fully to equilibrium before the first spectrum was recorded. The second group included Val31, Leu33, Leu53, Val91, and Val96. The signals from these residues were observed as two peaks during the exchange process. The respective chemical-shift differences for these peaks were 2.6, 3.2, 7.0, 2.2, and 6.1 Hz. The larger values for Leu53 and Val96 were indicative of the β shift, and the others were indicative of the γ shift. In this group, the only time-dependent effect arose from the amide hydrogen with the slow exchange rate, because the other exchange was too fast to detect. All of these amide hydrogens, except for Leu53, are located on the edges of a β sheet in SSI, and those at the γ and β sites do not participate in intramolecular hydrogen bonds. Although the amide hydrogens of both Leu33 and Thr34 form hydrogen bonds in the β sheet, the amide hydrogen from Thr34 exchanges very rapidly for reasons discussed in detail in the following section. The third group, which included the $^{13}\mathrm{C}'$ signals from Val13, Val16, Val31, Val78, Val85, and Leu80, displayed four peaks during the exchange. Because both of the neighboring amide hydrogens of these carbonyl carbons exchanged slowly, they allowed the measurement of both the uncorrelated and correlated exchange rates. All of these slowly exchanging amide hydrogens are located in the antiparallel five-stranded β sheet of SSI. The observed values of the β and γ shifts are
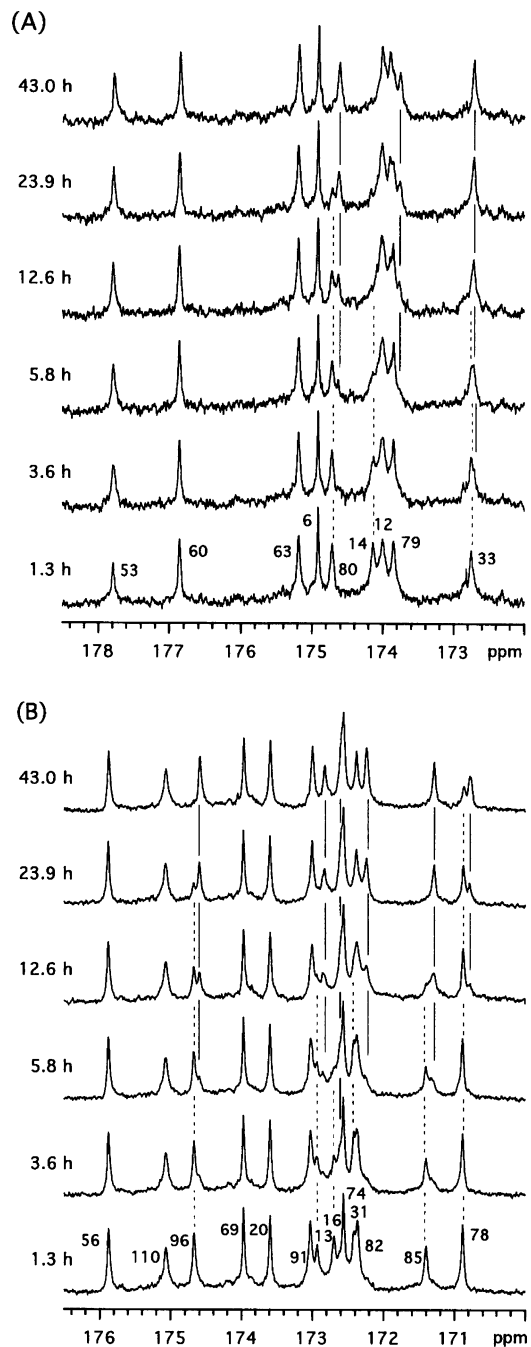
FIGURE 3: Time dependence of 75.4 MHz $^{13}\mathrm{C}$ NMR spectra of selectively labeled SSI samples at pH* 7.4 at various times following transfer of the protein from $\mathrm{H_2O}$ to $^2\mathrm{H_2O}$: (A) [L]SSI and (B) [V]SSI. The temperature of the samples was kept at 50 °C. Each spectrum represents the accumulation of 4096 transients of FID signals for 2.26 h. The $^{13}\mathrm{C}'$ resonance assignments are indicated by residue numbers at the bottom. Some of the resonances exhibited time-dependent spectral changes. The decrease in the peaks of [H,H] and the increase in the peaks of [D,D] are represented by broken and straight lines, respectively.

summarized in Table 1. At 75.4 MHz, the magnitudes of the β shifts were about 6–7 Hz and the γ shifts were 2 Hz or less. We also found that the magnitudes of these isotope shifts were independent of pH* in the range from 6 to 10.

To determine the exchange rates quantitatively, a total line-shape analysis was carried out. In the case of the resonances in which both of the isotope effects were observed, the exchange rates were determined, as described below. A

Table 1: β and γ Shift Values for Selected $^{13}C'$ Resonances in [L]SSI and [V]SSI[a]

residue	β shift (Hz)	γ shift (Hz)	residue	β shift (Hz)	γ shift (Hz)
Val13	6.1	2.5	Leu80	6.5	1.6
Val16	6.1	1.9	Val82	7.1	2.9
Val31	nd	2.6	Val85	6.1	2.3
Leu33	nd	3.2	Val91	nd	2.2
Leu53	7.0	nd	Val96	6.1	nd
Val78	6.6	1.9			

[a] All of the data were collected on a Varian XL-300 spectrometer (^{13}C frequency of 75.4 MHz) under the conditions of pH* 7.3 at 50 °C. These isotope shifts were found to be independent of pH* in the range from 6 to 10. The notation "nd" indicates that the isotope shift was not detected.
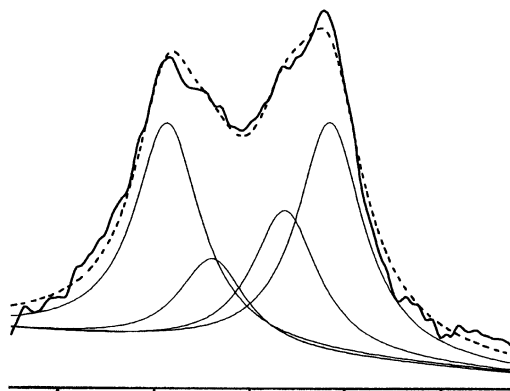

FIGURE 4: Line-shape analysis of the carbonyl resonance of Val85 of SSI acquired at 75.4 MHz at 50 °C and pH* = 7.8. The thick line represents the observed signal, which was accumulated for 10.26 h. The thin continuous lines indicate the signals corresponding to the four [i, $i + 1$] isotopomers: from left to right, [H,H], [D,H], [H,D], and [D,D]. The fitted spectrum obtained by adding the four subspectra is represented by the broken line. One division of the axis shows 10 Hz. The line-shape analysis was carried out with the constant values of 6.1, 2.3, and 8.3 Hz for the β shift, γ shift, and line width, respectively. The exchange rates determined by using appropriate initial values were $k_{\beta}' = 2.30 \times 10^{-3}$ min^{-1}, $k_{\gamma}' = 1.63 \times 10^{-3}$ min^{-1}, and $k_c = 6.38 \times 10^{-4}$ min^{-1} (see the text for details).

typical example is shown in Figure 4. The thick line shows the observed spectrum of Val85 at 50 °C and pH* 7.8. In this case, the spectrum was obtained by summing from the 1st to 18th subspectrum. Because each subspectrum was accumulated for 0.57 h, the accumulation period was 10.26 h. An initial dead time of 0.17 h was needed, for instrumentation preparation, such as probe tuning and shimming. The line-shape analysis was carried out using eqs 9–12, with $k_{\beta}' = 0.1$ min^{-1}, $k_{\gamma}' = 0.1$ min^{-1}, and $k_c = 0.1$ min^{-1} as the initial values, and the values of the β and γ shifts and the line widths of the four species were fixed as 6.1, 2.3, and 8.3 Hz, respectively. These fixed values were estimated from the summed spectrum and were finally determined by trial and error with the calculations. The baseline was corrected by a straight line. Because the convergences of the fitting calculation to the observed spectra were fast and stable after a few iterations, the initial values could be roughly estimated. We confirmed that several choices of appropriate initial values converged to the same values within the calculation errors. The broken line indicates the calculated spectrum, and the solid lines represent the individual [H,H], [D,H], [H,D], and [D,D] species. The results are summarized in Table 2.

Because the carbonyl resonances of Val31, Leu33, Leu53, Val91, and Val96 displayed only one of the isotope effects, their signals were analyzed by the two-site exchange model, which yielded one apparent exchange rate constant, k_{obs} (Table 2 and Figure 6). Because the carbonyl resonances of Leu12, Leu14, and Leu79 were heavily overlapped, we were unable to determine the exchange rates of these amide hydrogens. The logarithms of the apparent exchange rates (log k_{β} and log k_{γ}) and the fraction of correlated exchange ($X_{\beta\gamma}$) are plotted as a function of pH* in Figure 5.

All pairs of residues showed low fractions of correlated exchange at low pH but increased fractions at higher pH. Val13−Leu14, Val78−Leu79, Leu80−Thr81, and Val82−Asp83 achieved fractions of correlated exchange approaching 0.7−0.8 at high pH. However, the Val16−Gly17 and Val85−Trp86 pairs only achieved correlated exchange fractions of about 0.4 at high pH*.

DISCUSSION

Amide Groups Amenable to Investigation by the Approach Used Here. Native protein molecules are stabilized by many interactions, such as hydrogen bonds, hydrophobic and electrostatic interactions, and disulfide bonds, if present. Because the free energy for the stabilization of a native protein molecule is only about 10 kcal mol^{-1} (*38*), thermal fluctuations can affect the dynamic structure and function of proteins. The analysis of the exchangeable hydrogens, especially the backbone amide hydrogens, in a protein is one of the most important ways to study its dynamic features. Because contact with solvent molecules is necessary to exchange the buried amide hydrogens, some native interactions must be partially or fully broken.

Each SSI subunit contains two α helices and one five-stranded β sheet and some of the Leu and Val residues are distributed within these secondary structures. Amide hydrogens that are not involved in these secondary structures exchange very rapidly (Leu6, Tyr7, Val20, Ser21, Leu60, Asn61, Leu63, Thr64, Val69, Met70, Val74, and Try75). Amide hydrogens located at the edge of the β sheet and not participating in hydrogen bonding also displayed fast exchange (Thr32, Ser92, and Val96). The N-terminal region from Asp1 to Leu6 of SSI projects away from the globular part of the molecule and is mobile. The relative solvent accessibilities (Ra) of Leu6 and Tyr7 were determined to be 100% (*39*). Because this region is freely accessible to the solvent, regardless of the rest of the SSI molecule, the exchange rates may be as fast as those of small peptides. The high mobility of this region was also indicated by the narrow line width of the Leu6 resonance (Figure 3). The Ra values of some of the other fast exchanging amide hydrogens without secondary structures (Val20, Ser21, Asn61, Leu63, and Val74) were 0%; however, these amide hydrogens are located near the surface of the molecule and exchanged rapidly apparently as the result of local fluctuations. None of the exchange rates of these rapidly exchanging amides could be determined by the method employed here.

Those slowly exchangeable amides of SSI that could be investigated by the carbonyl ^{13}C NMR approach employing selective labeling of Leu and Val residues are listed in Table 1. Although the amide hydrogens of Leu12 and Thr15 were found to exchange slowly, as judged from the spectral

Table 2: H/D Exchange at Selected Sites in SSI 50 °C: Apparent Rates of Backbone Amide Hydrogen Exchange at Residues i and $i + 1$ (k_γ and k_β, Respectively), Apparent Rates of Correlated Exchange at the Two Sites (k_c), and Fraction of Exchange Occurring by the Correlated Mechanism ($X_{\beta\gamma}$)

residue i	pH*	k_β (min^{-1}) apparent rate of exchange by the noncorrelated mechanism at residue $i + 1$	k_γ (min^{-1}) apparent rate of exchange by the noncorrelated mechanism at residue i	k_c (min^{-1}) apparent rate of correlated exchange	$X_{\beta\gamma}$ fraction of exchange occurring by the correlated mechanism
Val13	7.4	1.40×10^{-3}	2.72×10^{-4}	2.48×10^{-4}	0.30
	7.8	2.84×10^{-3}	1.00×10^{-3}	8.92×10^{-4}	0.46
	8.6	9.27×10^{-3}	5.27×10^{-3}	4.57×10^{-3}	0.63
	9.1	8.52×10^{-3}	5.45×10^{-3}	4.20×10^{-3}	0.60
	9.5	1.03×10^{-2}	1.04×10^{-2}	7.55×10^{-3}	0.73
Val16	7.4[a]	3.25×10^{-3}	7.18×10^{-4}	1.08×10^{-11}	0.00
	7.8	6.22×10^{-3}	2.49×10^{-3}	6.70×10^{-4}	0.15
	8.6	7.98×10^{-3}	4.70×10^{-3}	2.38×10^{-3}	0.38
	9.1	1.20×10^{-2}	6.08×10^{-3}	2.72×10^{-3}	0.30
Val31[b]	6.1		3.20×10^{-4}		
	7.4		1.19×10^{-3}		
	7.8		1.65×10^{-3}		
	8.6		3.97×10^{-3}		
	9.1		9.20×10^{-3}		
	9.5		1.07×10^{-2}		
Leu33[b]	7.3		1.82×10^{-3}		
	8.0		3.72×10^{-3}		
	9.2		3.48×10^{-3}		
	9.4		5.18×10^{-3}		
	10.0		2.25×10^{-2}		
Leu53[b]	6.1	5.87×10^{-3}			
Val78	6.1	6.21×10^{-5}	2.00×10^{-5}	7.30×10^{-6}	0.18
	7.4	2.53×10^{-4}	7.87×10^{-5}	3.33×10^{-5}	0.20
	7.8	3.79×10^{-4}	1.62×10^{-5}	8.93×10^{-5}	0.33
	8.6	1.27×10^{-3}	9.55×10^{-4}	4.49×10^{-4}	0.40
	9.1	3.00×10^{-3}	1.76×10^{-3}	1.13×10^{-3}	0.48
	9.5	8.88×10^{-3}	6.86×10^{-3}	5.83×10^{-3}	0.74
	10.1	1.90×10^{-2}	1.17×10^{-2}	1.05×10^{-2}	0.69
Leu80	6.1	3.38×10^{-4}	1.11×10^{-4}	6.63×10^{-5}	0.30
	7.3[a]	8.02×10^{-4}	1.68×10^{-3}	3.27×10^{-11}	0.00
	8.0	1.77×10^{-3}	1.79×10^{-3}	5.35×10^{-4}	0.30
	9.4[a]	6.85×10^{-3}	4.80×10^{-3}	4.80×10^{-3}	0.82
	10.0	1.05×10^{-2}	6.73×10^{-3}	6.73×10^{-3}	0.78
Val82	6.1	2.78×10^{-4}	2.53×10^{-4}	2.80×10^{-5}	0.11
	7.4	1.10×10^{-3}	1.15×10^{-3}	3.52×10^{-5}	0.03
	7.8	2.13×10^{-3}	2.44×10^{-3}	1.03×10^{-3}	0.45
	8.6	3.35×10^{-3}	4.05×10^{-3}	2.75×10^{-3}	0.74
	9.1	6.30×10^{-3}	8.07×10^{-3}	5.37×10^{-3}	0.75
	9.5	9.36×10^{-3}	9.56×10^{-3}	8.25×10^{-3}	0.87
Val85	6.1	3.71×10^{-4}	2.78×10^{-4}	7.08×10^{-5}	0.22
	7.4	1.37×10^{-3}	1.06×10^{-3}	4.12×10^{-4}	0.34
	7.8	2.94×10^{-3}	2.27×10^{-3}	6.38×10^{-4}	0.25
	8.6	7.17×10^{-3}	5.80×10^{-3}	2.08×10^{-3}	0.32
	9.1	1.66×10^{-2}	2.54×10^{-2}	8.37×10^{-3}	0.40
Val91[b]	7.4		1.43×10^{-3}		
	7.8		3.62×10^{-3}		
	8.6		7.77×10^{-3}		
	9.1		1.39×10^{-2}		
	9.5		9.63×10^{-2}		
Val96[b]	7.8	1.66×10^{-3}			
	8.6	3.28×10^{-3}			
	9.1	7.03×10^{-3}			
	9.5	1.03×10^{-2}			

[a] These data may contain relatively large errors, because the S/N ratios of the observed resonances were low. [b] These data were analyzed by a two-site exchange model to determine the apparent exchange rates; because one of the isotope effects was not observed as a result of fast exchange, it was not possible to measure correlated exchange at these sites.

changes, the carbonyl resonances were overlapped and the exchange rates could not be determined. All of these amide hydrogens, except for those of Ala54, were localized in the five-stranded β sheet. Because the exchange rate of Ala54 was relatively fast, it was determined only at pH* 6.1; at higher pH* values, the rate was too fast to measure by this method. SSI is a dimeric protein with each subunit composed of a five-stranded β sheet, which is formed with an abundance of hydrophobic amino acid residues, including ca. 60% of Leu and Val residues. Most of the amide hydrogens of the β and γ sites of these Leu and Val residues participate in β-sheet hydrogen bonds (Figure 7). As shown in Figure 5, the exchange rates of these amide hydrogens depend on pH* and extend from 10^{-5} to 10^{-1} min^{-1} in the range of 6 < pH* < 10. Akasaka et al. (24) reported the 10

slowest exchanging amide hydrogens in SSI, and our results agree well with their data.

It is well-known that hydrogen-bond formation reduces amide exchange rates remarkably. Our results bear this out in general, but there are exceptions. The amide hydrogens of Gly17, Leu79, and Leu80 are located at the end of a β sheet, where the hydrogen-bond network as determined by X-ray analysis (39) is disordered. Although the amide hydrogen of Leu79 had one of the slowest exchange rates, it does not participate in any hydrogen bond. The five-stranded β sheets of the respective subunits of SSI face one other at an angle of approximately 30 °; therefore, the region of the β sheet bearing these amide hydrogens was not covered by another subunit. However, this part of the β sheet seems to be sequestered from the solvent by the loop structure from
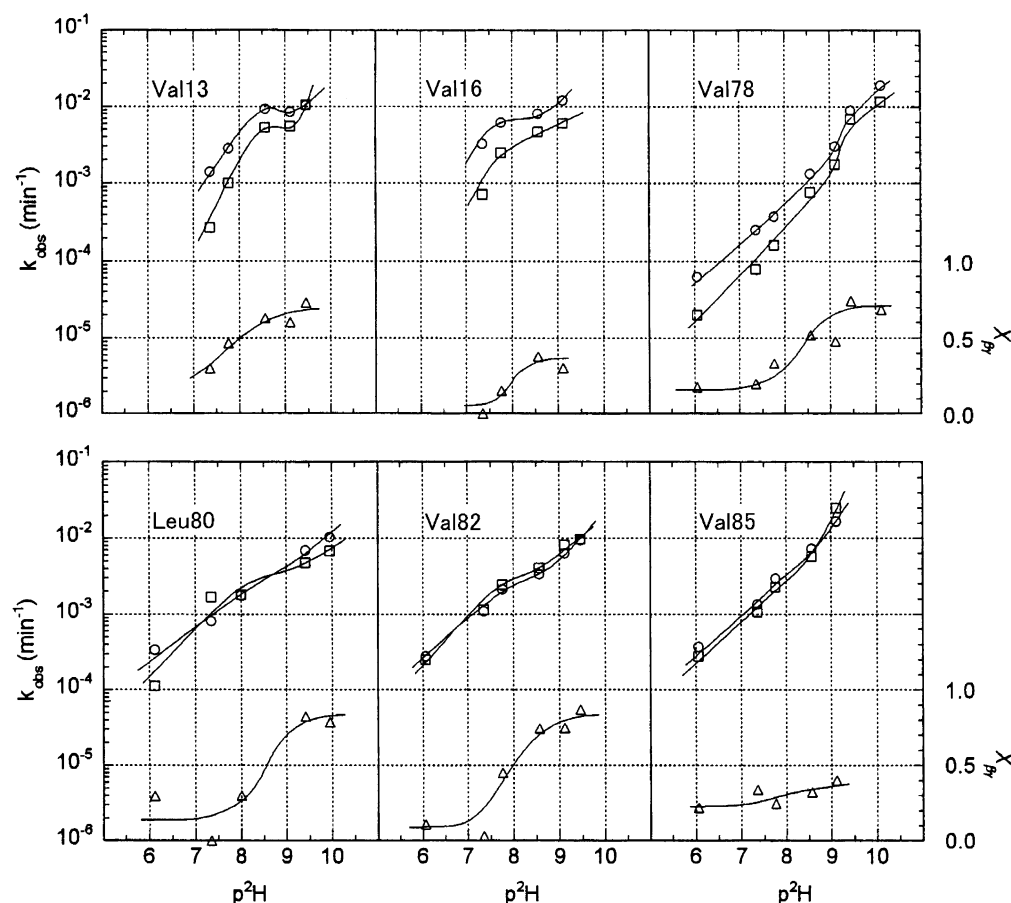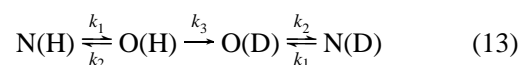
FIGURE 5: pH* dependence of the logarithm of the apparent H/D exchange rates (k_β and k_γ) of adjacent amides in SSI at 50 °C and the fraction of exchange occurring by the correlated mechanism ($X_{\beta\gamma}$). The residue whose carbonyl carbon ($^{13}C'_i$) was monitored is indicated in each panel. The open circles, squares, and triangles represent k_β, k_γ, and $X_{\beta\gamma}$, respectively (see the text for details).

Lys18 to Glu28. We also found that the amide hydrogen of Thr34 hydrogen bonded to the carbonyl oxygen of Ser40; however, the β shift on the carbonyl resonance of Leu33 was not observed over the entire pH* range. This means that exchange of the Thr34 amide hydrogen is very fast despite its participation in a hydrogen bond. The shortest strand (β3), which contains Ser40, is located at the edge of the β sheet and forms only three hydrogen bonds with strand β2. Therefore, one might expect that the interaction between these strands should be weak and that the hydrogen bond between Thr34 and Ser40 may easily break; however, this is one of the slowly exchanging sites. Similarly, Leu78, which is one of most slowly exchanging sites, is located in the region that includes Gly17, Leu79, and Leu80. We found that the exchange rate of Ala54 was relatively fast, even though it is located in the center of an α helix and forms a hydrogen bond. Similar anomalous exchange results have been reported for other proteins (*17, 18*). Zhang et al. (*28*) reported that the amide hydrogens located in the hydrophobic interface displayed slow exchange. Most of the slowly exchanging amide hydrogens in SSI are located in the hydrophobic interface of the subunit. Pederson et al. (*18*) discussed the exchange rates in terms of the factors of hydrogen bonding, types of secondary structure, and depth from the surface of the protein molecule. They concluded that all of the factors were important, but the exchange rates were not uniquely determined by any of these factors definitively.

Correlated Motions in SSI. It is widely accepted that fluctuations are required for the solvent exchange of amide hydrogens that are fully or partially buried within a protein molecule. The local unfolding model (*21, 22*) is one of the mechanisms by which the buried amide hydrogens can exchange. Two types of fluctuations can be envisioned. One is a local fluctuation that requires only a low activation energy. The other is a global fluctuation that induces a wider range of disorder in the protein molecule and requires larger activation energy. Both of these processes could coexist in actual proteins and facilitate the exchange of amide hydrogens. The exchange process in the local unfolding model is represented by the following equation (*40*)

$$N(H) \underset{k_2}{\overset{k_1}{\rightleftharpoons}} O(H) \overset{k_3}{\rightarrow} O(D) \underset{k_1}{\overset{k_2}{\rightleftharpoons}} N(D) \qquad (13)$$

where N represents the folded conformation. An internal amide hydrogen in a protein cannot exchange, because the solvent molecules do not have access to it. O indicates the unfolded state, in which the amide hydrogen can exchange. Because the native state of a protein favors the folded conformation, the equilibrium lies toward the N state, and then $k_1 \ll k_2$. In this situation, the exchange rate, k_{ex}, is represented by

$$k_{ex} = \frac{k_1 k_3}{k_1 + k_2 + k_3} \qquad (14)$$

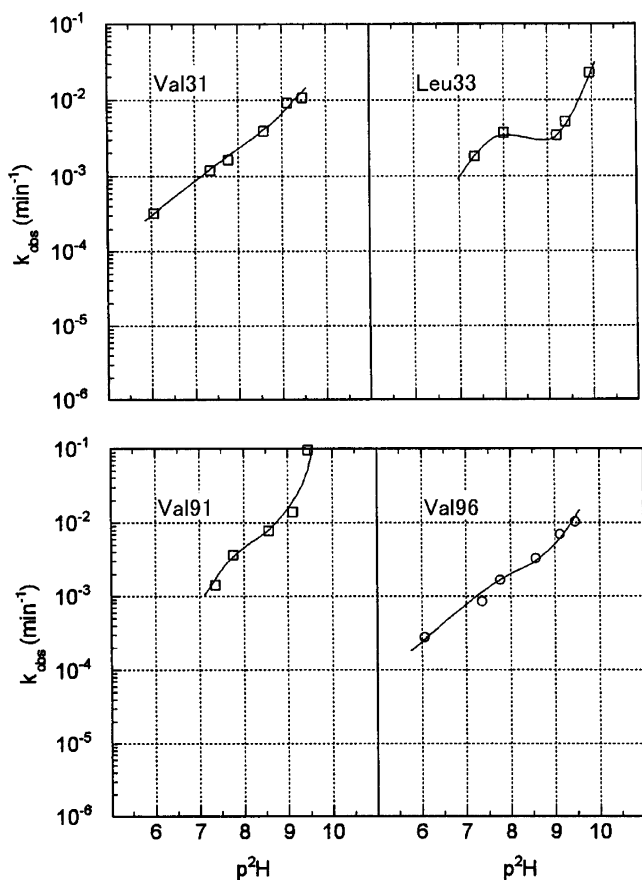FIGURE 6: pH* dependence of the logarithm of the apparent H/D exchange rates (k_β and k_γ) of adjacent amides in SSI at 50 °C. The residue whose carbonyl carbon ($^{13}C'_i$) was monitored is indicated in each panel. The open circles and squares represent k_β and k_γ, respectively. The line-shape analyses were carried out by the two-site exchange model, because the data did not support the determination of correlated exchange at these sites (see the text for details).

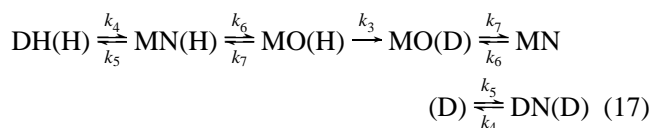When $k_1 \ll k_2$ and $k_2 \ll k_3$ (EX1 condition), the equation simplifies to

$$k_{ex} = k_1 \qquad (15)$$

Because the opening rate of the protein determines the exchange rate under these conditions, the exchange rate displays the internal fluctuation directly. On the other hand, when $k_1 \ll k_2$ and $k_3 \ll k_2$ (EX2 condition), the exchange rate is given by

$$k_{ex} = \frac{k_1}{k_2} k_3 = K k_3 \qquad (16)$$

where $K = k_1/k_2$. The exchange rates, k_3, are available (41, 42), and thus, the equilibrium constants for the individual amide hydrogens can be determined.

The exchange scheme is more complicated in the case of SSI, because SSI is a dimeric protein constructed from two identical subunits. The detailed exchange equation in the case of SSI is represented by

$$DH(H) \underset{k_5}{\overset{k_4}{\rightleftharpoons}} MN(H) \underset{k_7}{\overset{k_6}{\rightleftharpoons}} MO(H) \overset{k_3}{\rightarrow} MO(D) \underset{k_6}{\overset{k_7}{\rightleftharpoons}} MN$$

$$(D) \underset{k_4}{\overset{k_5}{\rightleftharpoons}} DN(D) \quad (17)$$

where DN, MN, and MO represent the folded state in the dimer, the folded state in the monomer, and the unfolded state in the monomer, respectively. However, it is known that the equilibrium between the dimer and the monomer extremely favors the dimer, and the dissociation constant is estimated to be lower than 5×10^{-7} M in SSI (34). Moreover, it has been reported on the basis of thermal (29, 43) and SDS (44) denaturation experiments that the monomeric form of SSI should be unfolded. These results indicate that $k_4 \ll k_5$ and $k_7 \ll k_6$, and thus, the concentration of the MN species would be very low. Therefore, the exchange scheme can be simplified to that of eq 13, which represents the case of a simple monomeric protein. We can discuss the amide hydrogen exchange on SSI without any special considerations because of dimeric protein.

The general approach used in distinguishing whether a given amide hydrogen exchanges by the EX1 or EX2 mechanism is to examine its pH dependence. Normally, the assumption is made that the unfolding equilibrium is pH-independent. In this case, the observed exchange rate is proportional to the catalyst concentration in the EX2 limit and independent of the catalyst concentration in the EX1 limit. Some methods for the direct detection of correlated exchange have been reported. For example, correlated exchange was detected in the β sheet of BPTI by analyzing the time dependence of NOEs between amide hydrogens; when normalized for single-site exchange rates, the NOE intensities of sites undergoing correlated exchange decreased more rapidly than those undergoing uncorrelated exchange (23, 26). Mass spectroscopic investigations have indicted that the amide hydrogens in lysozyme at pH 3.8 and 69 °C exchange predominantly by the EX2 mechanism (27). Mass spectrometry was used in detecting correlated exchange in aldolase (28).

In none of the previous investigations of correlated hydrogen exchange has a detailed analysis of the pH dependence of exchange been carried out. In principle, one expects in the EX2 limit that the correlated exchange rate will be much lower than the uncorrelated rate. In addition, whereas the uncorrelated rate in the EX2 limit depends on the catalyst concentration, in this limit, the correlated rate should depend on the square of the catalyst concentration. In the EX1 limit, both rates should be independent of catalyst concentration. The pH at which the transition from EX2 to EX1 occurs may be different for the uncorrelated and correlated exchange rates, depending on their relative magnitudes.

When the expected EX2 limit pH dependence is inserted into the rates, eq 8 becomes

$$X_{\beta\gamma} = 2k_c^\circ [OH^-]/(k_\beta^\circ + k_\gamma^\circ) \qquad (18)$$

where the zeroes indicate the pH-independent rates. Thus, one predicts that $X_{\beta\gamma}$ will be pH-dependent with a sigmoidal dependence as observed in Figure 5.

We have analyzed the data from Table 2 to extract the pH-independent rate constants for the single- and two-site correlated exchange. The best fits were for the data from the carbonyls of Val78 and Val85. Except for the pH 9.5 and 10.1 data points for Val78, the fitted rate constants when inserted into eq 18 provided reasonable approximations of the observed pH dependence of $X_{\beta\gamma}$ (Figure 5). The recon-
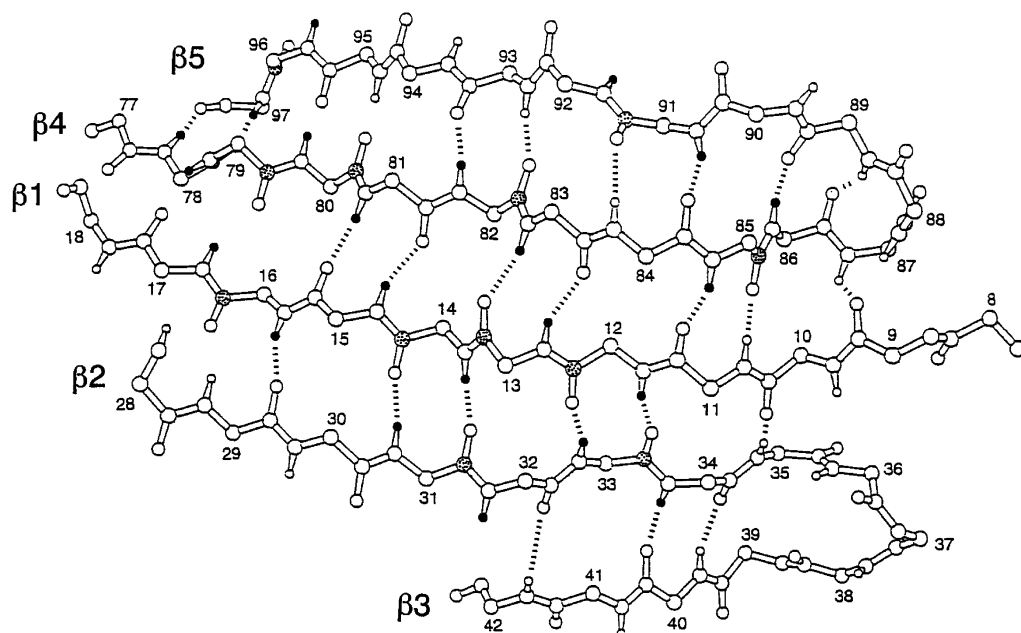
FIGURE 7: Schematic drawing of hydrogen-bonding network in the five-stranded antiparallel β sheet in SSI. The stippled atoms designate the carbonyl carbons of Leu and Val residues. The dashed lines represented hydrogen bonds determined by X-ray crystallography (*39*).

Table 3: Fitted Values for the pH-Independent Rate Constants Derived from Linear Regression Analysis of the Data from Table 2

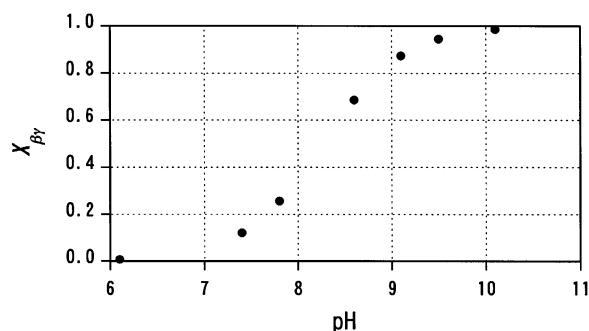|	$k_\beta{}^\circ$ (min^{-1} M^{-1})	r^2	$k_\gamma{}^\circ$ (min^{-1} M^{-1})	r^2	$k_c{}^\circ$ (min^{-1} M^{-2})	r^2
Val13	2.2×10^2	0.53	2.9×10^2	0.89	5.6×10^6	0.66
Val16	4.8×10^2	1.00	2.7×10^2	0.86	8.8×10^6	0.48
Val78	1.5×10^2	0.96	2.1×10^2	0.98	5.7×10^6	1.00
Leu80	9.6×10^1	0.86	5.6×10^1	0.80	5.3×10^6	0.63
Val82	2.7×10^2	0.91	2.8×10^2	0.82	7.2×10^6	0.75
Val85	1.2×10^3	0.99	2.0×10^3	0.99	5.0×10^7	0.98

FIGURE 8: Simulated plot of $X_{\beta\gamma}$ versus pH according to eq 18. The pH-independent exchange rate constants used in the simulation were $k_\beta{}^\circ = 1.5 \times 10^2$ M^{-1} min^{-1}, $k_\gamma{}^\circ = 2.1 \times 10^2$ M^{-1} min^{-1}, and $k_c{}^* = 5.7 \times 10^6$ M^{-2} min^{-1} (Table 3). These values were estimated from fitting the experimental data for Val78 (Table 2).

structed pH dependence of $X_{\beta\gamma}$ is shown in Figure 8. Our analysis assumes that

$$\frac{k_1}{k_2} = K \qquad (19)$$

is independent of pH. In the case of SSI, this assumption should be satisfied, because SSI is a very stable protein and its native structure persists even at pH 13.3 and 25 °C or pH 12.2 and 50 °C (*45*). The results of this study can be explained by the exchange occurring in the EX2 limit, including two-site correlated exchange. We provide, for the

first time, an analysis of the rates of correlated exchange at two adjacent peptide amides.

The amide pairs in SSI shown here to undergo correlated exchange at high pH are located in antiparallel β sheet and participate in hydrogen bonds (Figure 7). The amide hydrogens of adjacent residues in a β strand project toward opposite sides and form hydrogen bonds with opposite strands. Therefore, correlated exchange of these amide hydrogens implies global unfolding that involves all three β strands. Because the five-stranded β sheet forms the interface of the dimer, this transition must also involve the dissociation of SSI to monomers.

ACKNOWLEDGMENT

REFERENCES

1. Karplus, M., and McCammon, J. A. (1981) The internal dynamics of globular proteins, *CRC Crit. Rev. Biochem. 9*, 293−349.

2. Linderstrom-Lang, K. (1955) Deuterium exchange between peptides and water, *Chem. Soc. Spec. Publ. 2*, 1−20.

3. Woodward, C., Simon, I., and Tuchsen, E. (1982) Hydrogen exchange and the dynamic structure of proteins, *Mol. Cell. Biochem. 48*, 135−160.

4. Englander, S. W., and Kallenbach, N. R. (1984) Hydrogen exchange and structural dynamics of proteins and nucleic acids, *Q. Rev. Biophys. 16*, 521−655.

5. Englander, S. W., and Mayne, L. (1992) Protein folding studied using hydrogen-exchange labeling and two-dimensional NMR, *Annu. Rev. Biophys. Biomol. Struct. 21*, 243−265.

6. Baldwin, R. L. (1993) Pulsed H/D-exchange studies of folding intermediates, *Curr. Opin. Struct. Biol. 3*, 84−91.

7. Bai, Y., Sosnick, T. R., Mayne, L., and Englander, S. W. (1995) Protein folding intermediates: Native-state hydrogen exchange, *Science 269*, 192−197.

8. Krishna, M. M. G., Hoang, L., Lin, Y., and Englander, S. W. (2004) Hydrogen exchange methods to study protein folding, *Methods 34*, 51−64.

9. Mayne, L., Paterson, Y., Cerasoli, D., and Englander, S. W. (1992) Effect of antibody binding on protein motions studied by hydrogen-exchange labeling and two-dimensional NMR, *Biochemistry 31*, 10678−10685.

10. Zahn, R., Spitzfaden, C., Ottger, M., Wüthrich, K., and Pluckthun, A. (1994) Destabilization of the complete protein secondary structure on binding to the chaperone GroEL, *Nature 368*, 261−265.

11. Reid, C. W., Brewer, D., and Clarke, A. J. (2004) Substrate binding affinity of *Pseudomonas aeruginosa* membrane-bound lytic trans-glycosylase B by hydrogen−deuterium exchange MALDI MS, *Biochemistry 43*, 11275−11282.

12. Loftus, D., Gbenle, G. O., Kim, P. S., and Baldwin, R. L. (1986) Effects of denaturants on amide proton exchange rates: A test for structure in protein fragments and folding intermediates, *Biochemistry 25*, 1428−1436.

13. Englander, J. J., Calhoun, D. B., and Englander, S. W. (1979) Measurement and calibration of peptide group hydrogen−deuterium exchange by ultraviolet spectrophotometry, *Ann. Biochem. 92*, 517−524.

14. Harmen H. J., de Jong, H., H., Goormaghtigh, E., and Ruysschaert, J.-M. (1985) Tertiary stability of native and methionine-80 modified cytochrome *c* detected by proton−deuterium exchange using online Fourier transform infrared spectroscopy, *Biochemistry 34*, 172−179.

15. Wagner, G., and Wüthrich, K. (1979) Structural interpretation of the amide proton exchange in the basic pancreatic trypsin inhibitor and related proteins, *J. Mol. Biol. 134*, 75−94.

16. Wagner, G., and Wüthrich, K. (1982) Amide protein exchange and surface conformation of the basic pancreatic trypsin inhibitor in solution. Studies with two-dimensional nuclear magnetic resonance, *J. Mol. Biol. 160*, 343−361.

17. Kossiakoff, A. A. (1982) Protein dynamics investigated by the neutron diffraction−hydrogen exchange technique, *Nature 296*, 713−721.

18. Pederson, T. G., Sigurskjold, B. W., Anderson, K. V., Kjaer, M., Poulsen, F. M., Dobson, C. M., and Redfield, C. (1991) A nuclear magnetic resonance study of the hydrogen-exchange behaviour of lysozyme in crystals and solution, *J. Mol. Biol. 218*, 414−426.

19. Lumry, R., and Rosenberg, A. (1975) The mobile defect hypothesis of protein function, *Coll. Int. C.N.R.S. L'Eau. Syst. Biol. 246*, 55−63.

20. Richards, F. M. (1979) Packing defects, cavities, volume fluctuations, and access to the interior of proteins, *Carsberg Res. Commun. 44*, 47−63.

21. Englander, S. W., and Mauel, C. (1972) Hydrogen exchange studies of respiratory proteins. II. Detection of discrete, ligand-induced changes in hemoglobin, *J. Biol. Chem. 247*, 2387−2394.

22. Englander, S. W., Calhoun, D. B., Englander, J. J., Kallenbach, N. R., Leim, R. H., Malin, E. L., Mandal, C., and Rogero, J. R. (1980) Individual breathing reactions measured in hemoglobin by hydrogen exchange methods, *Biophys. J. 32*, 577−589.

23. Roder, H., Wagner, G., and Wüthrich, K. (1985) Individual amide proton exchange rates in thermally unfolded basic pancreatic trypsin inhibitor, *Biochemistry 24*, 7396−7407.

24. Akasaka, K., Inoue, T., Hatano, H., and Woodword, C. K. (1985) Hydrogen exchange kinetics of core peptide protons in *Streptomyces* subtilisin inhibitor, *Biochemistry 24*, 2973−2979.

25. Kawata, Y., Goto, Y., Hamaguchi, K. Hayashi, F., Kobayashi, Y., and Kyogoku, Y. (1988) Hydrogen-exchange kinetics of the indole NH proton of the buried tryptophan in the constant fragment of the immunoglobulin light chain, *Biochemistry 27*, 346−350.

26. Wagner, G. (1980) A novel application of nuclear Overhauser enhancement (NOE) in proteins: Analysis of correlated events in the exchange of internal labile protons, *Biochim. Biophys. Rev. Commun. 97*, 614−620.

27. Miranker, A., Robinson, C. V., Radford, S. E., Aplin, R. T., and Dobson, C. M. (1993) Detection of transient protein folding populations by mass spectrometry, *Science 262*, 896−900.

28. Zhang, Z., Post, C. B., and Smith, D. L. (1996) Amide hydrogen exchange determined by mass spectrometry: Application to rabbit muscle aldolase, *Biochemistry 35*, 779−791.

29. Kainosho, M., and Tsuji, T. (1982) Assignment of the three methionyl carbonyl carbon resonances in *Streptomyces* subtilisin inhibitor by a carbon-13 and nitrogen-15 double-labeling technique. A new strategy for structural studies of proteins in solution, *Biochemistry 21*, 6273−6279.

30. Kainosho, M., Nagao, H., and Tsuji, T. (1987) Local structural features around the C-terminal segment of *Streptomyces* subtilisin inhibitor studied by carbonyl carbon nuclear magnetic resonances three phenylalanyl residues, *Biochemistry 26*, 1068−1075.

31. Uchida, K., Miyake, Y., and Kainosho, M. (1991) Reductive cleavage and regeneration of the disulfide bonds in *Streptomyces* subtilisin inhibitor (SSI) as studied by the carbonyl ^{13}C NMR resonances of cysteinyl residues, *J. Biomol. NMR 1*, 49−64.

32. Markley, J. L., and Kainosho, M. (1993) Stable isotope labeling and resonance assignments in larger proteins, in *NMR of Macromolecules* (Roberts, G. C. K., Ed.) pp 101−152, Oxford University Press, New York.

33. Hansen, P. E. (1983) Isotope effects on nuclear shielding, *Annu. Rep. NMR Spectrosc. 15*, 105−234.

34. Akasaka, K., Fujii, S., Hayashi, F., Rokushika, S., and Hatano, H. (1982) A novel technique for the detection of dissociation−association equilibrium in a highly associable macromolecular system, *Biochem. Ind. 5*, 637−642.

35. Hiromi, K., Akasaka, K., Mitsui, Y., Tonomura, B., and Murao, S. (1985) *Protein Protease Inhibitor−The Case of Streptomyces Subtilisin Inhibitor (SSI)*, Elsevier, Amsterdam, The Netherlands.

36. Nakanishi, M., and Tsuboi, M. (1976) Structure and fluctuation of a *Streptomyces* subtilisin inhibitor, *Biochim. Biophys. Acta 434*, 365−376.

37. Marquardt, D. W. (1963) An algorithm for least squares estimation of nonlinear parameters, *J. Soc. Ind. Appl. Math. 11*, 431−441.

38. Goto, Y., and Hamaguchi, K. (1979) The role of the intrachain disulfide bond in the conformation and stability of the constant fragment of the immunoglobulin light chain, *J. Biochem. 86*, 1433−1441.

39. Mitsui, Y., Satow, Y., Watanabe, Y., and Iitaka, Y. (1979) Crystal structure of a bacterial protein proteinase inhibitor (*Streptomyces* subtilisin inhibitor) at 2.6 Å resolution, *J. Mol. Biol. 131*, 697−724.

40. Havdt, A., and Nielsen, S. O. (1966) Hydrogen exchange in proteins, *Adv. Protein Chem. 21*, 287−386.

41. Molday, R. S., Englander, S. W., and Kallen, R. G. (1972) Primary structure effects on peptide group hydrogen exchange, *Biochemistry 11*, 150−158.

42. Bai, Y., Milne, J. S., Mayne, L., and Englander, S. W. (1993) Primary structure effects on peptide group hydrogen exchange, *Proteins 17*, 75−86.

43. Komiyama, T., Miwa, M., Yatabe, T., and Ikeda, H. (1984) A circular dichroism study on thermal denaturation of a dimeric globular protein, *Streptomyces* subtilisin inhibitor, *J. Biochem. 95*, 1569−1575.

44. Akasaka, K. (1984) Molecular strategy for the active conformation of *Streptomyces* subtilsin inhibitor, *Biomed. Res. 25* (supplement), 177−186.

45. Akasaka, K. Proton magnetic resonance spectra of a new proteinase inhibitor, *Streptomyces* subtilisin inhibitor (SSI) at 360 MHz. General characteristic and tyrosine titrations, in *Proceedings of the European Conference on NMR of Macromolecules* (Conti, F., Ed.) pp 475−483, Lerici, Rome, Italy.